Available online at www.sciencedirect.com

SciVerse ScienceDirect

Journal of the European Ceramic Society 32 (2012) 2949–2956

www.elsevier.com/locate/jeurceramsoc

Influence of Yb and Si content on the sintering and phase changes of Yb:YAG laser ceramics

Jan Hostaša [a,b,*], Laura Esposito [b], Andreana Piancastelli [b]

[a] Department of Glass and Ceramics, Institute of Chemical Technology, Prague, Technická 5, 166 28 Prague 6, Czech Republic
[b] ISTEC CNR, Institute of Science and Technology for Ceramics, Via Granarolo 64, 48018 Faenza, Italy

Available online 22 March 2012

Abstract

Yb-doped yttrium aluminum garnet (Yb:YAG) ceramics were prepared via solid state reaction of oxide powders. The Yb concentration ranged from 0 to 10 at.%. Silicon in the form of tetraethyl orthosilicate (TEOS) was added as a sintering aid in amounts of 0.3 and 0.5 wt.% with respect to the weight of solid. Thermal analyses (high temperature XRD, TG-DSC, dilatometric analyses) were performed on various compositions. Sintering was conducted under high vacuum and clean atmosphere. The influence of TEOS addition and Yb content was observed both in connection with phase transformations in function of temperature, and with microstructure and properties of sintered materials.

Keywords: Microstructure-final; Optical properties; Powders-solid state reaction; Sintering; YAG

1. Introduction

Transparent ceramics have drawn consistent attention in the last decades both as materials for armor applications or windows for aggressive environment or high temperatures, and as a possible replacement for single crystals.[1] The use of transparent yttrium aluminum garnet (YAG) ceramics is mainly focused on the last mentioned, i.e. the preparation of rare-earth doped YAG, namely laser active materials (Nd^{3+}, Yb^{3+}, Er^{3+}),[2–7] scintillators (Ce^{3+}), phosphors (Cr^{3+}, Tb^{3+}) or light converters for LED (Ce^{3+}, Eu^{3+}).[8,9] In the case of laser applications, the most used YAG dopant is Nd, and recently, with larger use of high-power InGaAs pumping diodes, the attention moved to Yb-doped infrared lasers[2,3] both for high power and ultra fast femtosecond lasers.[4,5] The Yb:YAG absorbs at wavelengths between 900 and 980 nm and emits at 1031 nm.[6]

Yb:YAG allows high doping (significantly higher than Nd:YAG) due to its simple electronic structure and low thermal problems thanks to small quantum defect. In the area of Yb:YAG ceramics for lasers there has been a number of papers focused on their preparation and use, also as single crystal–ceramics composite[10] or co-doped with other elements, e.g. Er[7] or Cr.[11]

In recent literature the role of the active elements on the sintering behavior and kinetics was reported.[12–14] It was shown that the active element may or may not enhance the sintering, depending on the size of the ion and its electronic structure.

This paper describes the preparation of Yb:YAG ceramics and studies both the solid state reactions occurring in the system, and the sintering in dependence on dopant content and on the amount of sintering aid (TEOS). We aim to provide basis for the further preparation of Yb:YAG, especially with higher Yb concentrations, by identifying the crucial factors in preparation of these materials in particular the role of the active elements and sintering aids during the thermal treatment.

2. Material and methods

Samples were prepared by reactive sintering of high-purity commercial oxide powders. The powders used and their characteristics are listed in Table 1.

Oxide powders were mixed in a stoichiometric ratio to produce $Y_3Al_5O_{12}$, in the case of Yb-doped samples, part of the yttria was substituted by equal (mol.) amount of ytterbia, providing the final composition $Y_{3-x}Yb_xAl_5O_{12}$. Weight loss of powders during sintering was taken into account as described in.[15] The homogenization was performed by ball milling for

* Corresponding author at: ISTEC CNR, Institute of Science and Technology for Ceramics, Via Granarolo 64, 48018 Faenza, Italy. Tel.: +39 0546 699723, fax: +39 0546 46381.
E-mail address: Jan.Hostasa@vscht.cz (J. Hostaša).

0955-2219/$ – see front matter © 2012 Elsevier Ltd. All rights reserved.
doi:10.1016/j.jeurceramsoc.2012.02.045

Table 1
Characteristics of commercial oxide powders.

Powder	Producer, type	S.S.A. [m^2/g]	D50 [μm]	Purity [%]	XRD phases	Main impurities [ppm]
Al_2O_3	Taimei, DS-6	17.22	0.20	>99.99	Al_2O_3	Si 3; Fe 7;Ca 2; Na, K, Mg 1
Y_2O_3	Nanocerox	45.2	0.05	>99.99	Y_2O_3	Na 35; Al 7; Si 60; S 40; P 10; Cl 80; Ca 10; Fe 8
Yb_2O_3	Alfa Aesar, REacton®	–	5.64	>99.99	Yb_2O_3	CaO 60; Fe_2O_3 3

72 h at 40 rpm in polyethylene bottles with alumina balls (99.99% Al_2O_3, diameter approx. 1 cm) in absolute ethanol; the powder:solvent:milling media weight ratio was 1:5:2. Organic dispersant (either PEG 400; or KM 5104, polyalkylene glycol from Zschimmer & Schwarz, Germany) was added to the mixture, and tetraethyl orthosilicate (TEOS) was added as a sintering aid in amounts of 0.3 and 0.5 wt.% with respect to the mass of powder). Table 2 summarizes the compositions of prepared mixtures.

The mixed suspensions were dried using a spray dryer (Mini Spray Dryer B-290, Büchi Labortechnik AG, Switzerland; equipped with Inert Loop B295 for organic solvent removal) under the following conditions: nozzle diameter 0.7 mm, feed rate 3 ml/min, argon flow rate 450 l/h, inlet temperature 70 °C and aspirator rate 70%. A thorough description of the spray drying conditions was reported elsewhere.[16] Spray dried powders were then formed into pellets by uniaxial pressing and cold isostatically pressed at 250 MPa.

Pressed samples were calcined for 24 h at 800 °C with temperature rise 20 °C/h until 800 °C or 100 °C/h until 300 °C, then 50 °C/h until 600 °C and 100 °C/h until 800 °C in order to achieve full removal of any organic substances. Sintering was performed under high vacuum (10^{-6} mbar) in a clean furnace with chamber and heating elements made of molybdenum and tungsten. The soaking times were 2 h, 8 h, 16 h at 1735 °C. The temperature selection was based upon previous results.[15]

Because samples sintered in vacuum contained oxygen vacancies (causing slightly gray coloration of samples) and Yb^{2+} ions (green coloration), they were treated by annealing in air. Annealing temperatures ranged from 1000 to 1100 °C and times differed with respect to dopant content and microstructure. Sintered and annealed samples were polished on silk plates with diamond pastes down to 0.25 μm. The microstructure and composition of sintered samples were investigated by scanning electron microscopy (SEM) (Leica Cambridge Stereoscan 360) coupled with an energy-dispersive X-ray spectrometer (EDX), by environmental scanning electron microscopy (ESEM; LEO 438 VP) and by optical microscope (Leica 301-371.011). Grain size was calculated by image analysis of microphotographs of polished (by ESEM) or polished and thermally etched samples (SEM or optical microscope) via the linear intercept method (approximately 200 grains were counted for each sample).

Theoretical density of Yb:YAG was calculated by linear fitting of the lattice parameters published in.[17,18] It has to be noted that the lattice parameters of YAG change with deviations from stoichiometry,[19] thus leading also to changes in theoretical density values.

Optical transmittance of polished samples was measured on an UV–vis spectrophotometer (Lambda 35 UV/Vis, PerkinElmer, USA) with 0.5 mm slit.

Selected powders were analyzed by high temperature XRD (D8 Advance BRUKER equipped with MRI TC BASIC), heating rate 10 °C/min, and TG/DTA (Model SAT 1500, PL Thermal Science), heating rate 10 °C/min in air, up to 1400 °C in order to provide information about the temperatures of phase formations. Dilatometry measurements (DIL 402 E, Netzsch–Gerätebau GmbH, Germany), heating rate 10 °C/min in air up to 1550 °C were performed on samples of representative compositions.

3. Theory

During the solid state reaction of alumina and yttria, intermediate phases are formed - the monoclinic ($Y_4Al_2O_9$, YAM) and hexagonal or orthorhombic perovskite ($YAlO_3$, YAP), before the high-temperature cubic garnet ($Y_3Al_5O_{12}$, YAG) appears.[20] The main reactions are listed in Eqs. (1)–(3).

$$2Y_2O_3 + Al_2O_3 \rightarrow Y_4Al_2O_9 \quad (1)$$

$$Y_4Al_2O_9 + Al_2O_3 \rightarrow 4YAlO_3 \quad (2)$$

$$3YAl_3 + Al_2O_3 \rightarrow Y_3Al_5O_{12} \quad (3)$$

Temperatures, at which these reactions occur, differ throughout literature. These variations can be explained both by different measurement techniques and conditions, and by the presence of impurities or doping ions. Moreover, as was mentioned in

Table 2
Compositions of prepared mixtures.

Composition	Yb [at.%]	TEOS [wt.%]	Dispersant [type, wt.%]
1	0	0.5	KM 5104, 1%
2	1	0.5	PEG, 1%
3	5	0.3	KM 5104, 1%
4	5	0.5	KM 5104, 1%
5	10	0.3	KM 5104, 1%
6	10	0.5	KM 5104, 1%
7	10	0.5	PEG, 1%

Table 3
Temperatures of phase formation obtained from high-temperature XRD (in °C).

Phase	Composition 1	Composition 4	Composition 6
$Y_4Al_2O_9$ (YAM)	1050	1050	1050
$YAlO_3$ (YAP)	1200	1150	1200
$Y_3Al_5O_{12}$ (YAG)	1350	1250	1300

Section 2, numerous equations leading to non-stoichiometric compounds may occur.[19]

In the case of Yb:YAG ceramics, the Yb^{3+} dopant ions substitute the Y^{3+} in the crystal lattice and give rise to intermediate compounds and eventually to full substitution leading to $Yb_3Al_5O_{12}$ (YbAG), which is isostructural to YAG. Compared to reactions (1)–(3) describing the presence of YAM and YAP phases, however,[21] reports no similar intermediate phases during polycrystalline YbAG preparation.

As was presented in the works of Ikesue and others,[22,23] the production of transparent YAG ceramics requires the use of sintering aid (viz. TEOS) for achieving sufficiently low residual porosity. The smaller (0.026 nm) Si^{4+} ions replace the Al^{3+} ions (0.039 nm) in the crystal structure of YAG.[24] The effect of silica addition to Nd:YAG system was already studied in various works.[22,23,25] Wen et al.[26] show the effect of silica addition (0.05, 0.5 and 3 wt.% of TEOS) for pure[1] YAG with following results: in the case of low amount of silica (0.05 wt.% of TEOS) the microstructure was porous with intergranular pores and relatively small grains. On the other hand, in the case of 3 wt.% precipitates appeared at grain boundaries. The addition of 0.5 wt.% of TEOS led to the elimination of pores without any reported presence of secondary phases, and thus was selected by the authors.

The effect of rare earth ions doping on sintering, microstructure and properties is also important. Papers have been published describing the supporting effect of Nd^{3+} doping on the sintering process.[25] It was also reported that in the case of Nd:YAG ceramics the Nd^{3+} ions tend to segregate at grain boundaries and slow the coarsening of microstructure, probably due to the solute drag effect.[25] Concerning Yb:YAG, in contrast to Nd^{+3}, the Yb^{3+} ions are smaller than Y^{3+} (ionic radii of Nd^{3+}, Y^{3+} and Yb^{3+} reported in literature are 1.0 Å, 0.89 Å and 0.86 Å, respectively,[27] or 1.109 Å, 1.011 Å and 0.985 Å, respectively, for 8-fold coordination [28]), and the substitution of Yb induces strain in crystal lattice due to the ion size. The grain boundary segregation of Yb^{3+} ions was not reported in literature, although grain boundary diffusion coefficient of both Nd and Yb is about 5 orders of magnitude higher than the bulk diffusion coefficient.[23]

The optical properties of transparent ceramics depend on losses due to scattering during light propagation,[29] either on pores, grain boundaries, secondary phases or impurities. In the case of YAG ceramics, when the grain boundaries are clean, they do not cause problems, because of the optical isotropy of the material. Main problem are the pores, because the difference in refractive indices is relatively high. Among the phases which may appear in the microstructure apart from YAG (n(YAG) = 1.815)[30] are aluminium and yttrium oxides ($n(Al_2O_3)$ = 1.760,[30] $n(Y_2O_3)$ = 1.915)[31] and YAP (n(YAP) = 1.96)[30] phase. The presented values show that the presence of YAP inclusions would cause more scattering than alumina. Other phases, which may appear in the microstructure, are alumina-, yttria- and ytterbia-silicates.

4. Results

4.1. Heat treatment in air (dilatometric, TG-DTA and high temperature XRD analyses)

The high temperature XRD analyses show that the amount of Yb influences the reaction temperature of the mixed oxides (Table 3). In sample containing 5 at.% of Yb the YAP and YAG phases start to form at lower temperature compared to samples containing 0 and 10 at.% Yb. In addition, the comparison of diffractograms reveals that at 1400 °C the composition with 5 at.% of Yb contained YAG as the main phase, while in the case of 10 at.% doping the amount of YAG was still very limited (Fig. 1).

The dilatometric analyses show that the composition with 5 at.% Yb exhibits a larger shrinkage compared to compositions with 0 and 10 at.% Yb, see Fig. 2.

The TG analyses of the three compositions (not reported) are very similar and do not show any consistent weight loss besides the one occurring in the range 200–400 °C related to the elimination of the organic component (dispersant).

In the DTA analysis of all the three powders an exothermic peak occurred at around 1200 °C (Fig. 3). This peak confirms what was already observed by the high temperature XRD analyses, i.e. the YAM and YAP phases form around 1200 °C. A second peak can be observed especially in the DTA curve of the pure YAG composition. This peak is not very well defined, because, according to the high temperature XRD analyses, the YAG phase starts to form when the YAP phase is still forming, and the two contributions are difficult to separate. In the case of the composition containing 10 at.% Yb the peak of the YAG phase can be barely observed, because even though this phase starts to form at 1300 °C (Table 3), at 1400 °C its amount is still very limited, as shown by the XRD patterns in Fig. 1.

The XRD and DTA do not highlight any consistent difference among the compositions prepared with a different or no dispersant or with 0.3 wt.% of TEOS instead of 0.5%.

[1] *Pure* here refers to the dopant content, thus with 0% Yb. The composition still contains sintering aid.

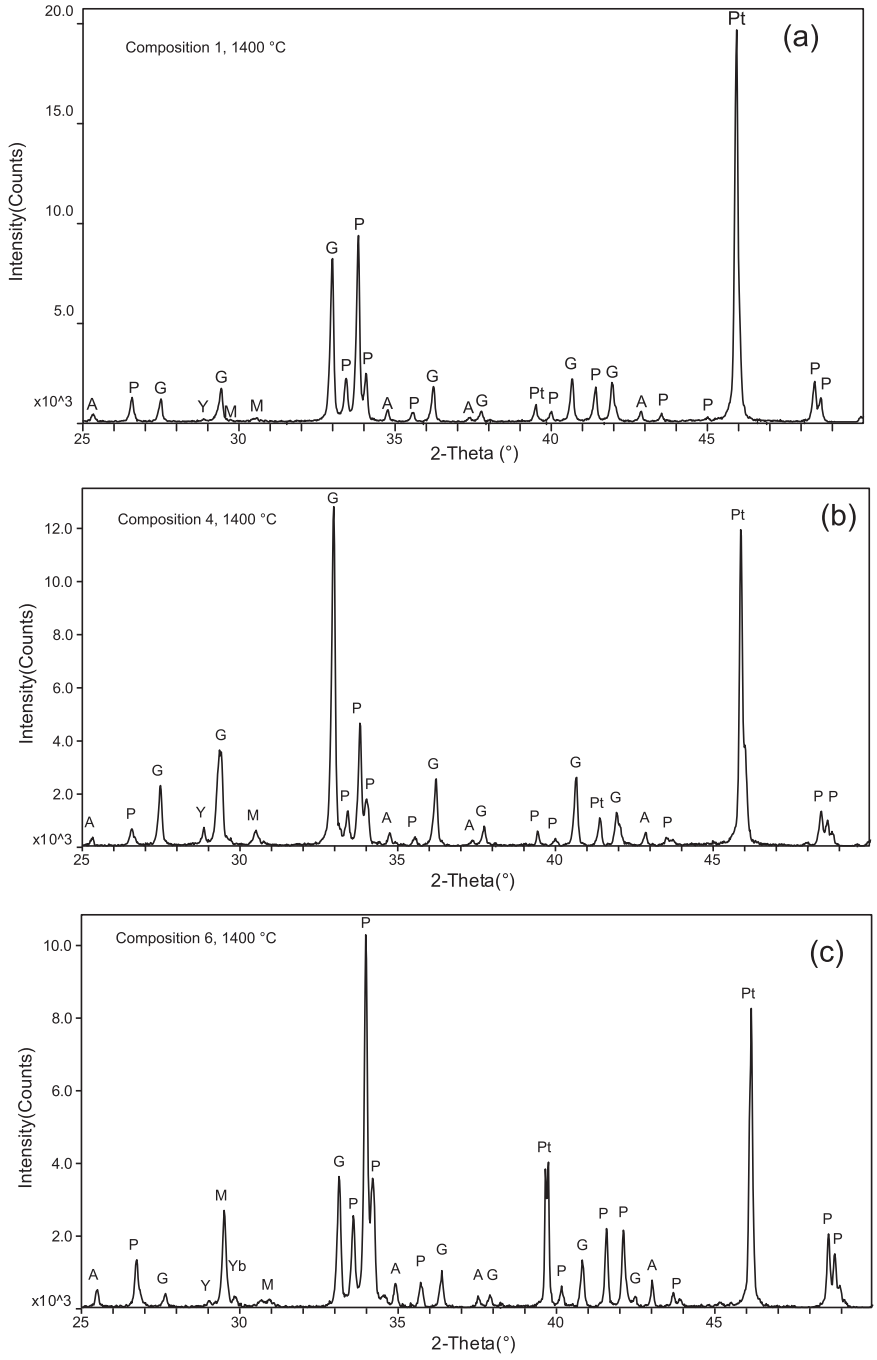

Fig. 1. XRD spectra of compositions (a) 1, (b) 4 and (c) 6 obtained at 1400 °C; A = alumina, Y = yttria, Yb = ytterbia, M = YAM, P = YAP, G = YAG, Yb:G = Yb:YAG.

4.2. Microstructural analyses: the grain size

The SEM, ESEM, optical microscope analyses and XRD spectra of all sintered samples show that the only phase present after sintering is YAG.

In Figs. 4 and 5 the microstructure of selected samples obtained using different analytical techniques is shown. The ESEM analysis is the least invasive technique since no additional treatment is required after surface polishing. ESEM enables to highlight the grains of materials thanks to their different orientation within the microstructure. However if contiguous grains have a similar or same orientation, this information is lost. The optical microscope analysis of samples after thermal etching allows a fast investigation of large areas of the samples but does not permit very high magnification. Finally, SEM analysis of thermally etched samples allows a complex characterization. Thermal etching, however, may promote some side effects, such as the formation of an amorphous phase that segregates at the grain boundary. A thorough microstructural characterization requires therefore the use of multiple analytical techniques.

Under the same sintering cycle of 16 h, compositions with no or 5 and 10 at.% Yb exhibit an average grain size of around 20 μm (Table 4, Figs. 4b and c and 5a and b). The grain size did

Table 4
Properties of sintered samples.

Composition	Sample	Yb content [at.%]	TEOS Content [wt.%]	Sintering cycle [°C × h]	Annealing [°C × h]	Grain size [μm]	RIT [%]
1	1-1	0	0.5	1735 × 8	1100 × 100	21.8	73.5
1	1-2	0	0.5	1735 × 16	1100 × 100	7.1 and 25.7[a]	72.0
2	2-1	1	0.5	1735 × 16	1300 × 0.5, 1000 × 100	28.5	80.9
3	3-1	5	0.3	1735 × 16	1100 × 100	21.4	57.0
4	4-1	5	0.5	1735 × 16	1100 × 100	19.7	68.5
5	5-1	10	0.3	1735 × 16	1050 × 400	16.4	71.0
6	6-1	10	0.5	1735 × 2	1050 × 300	13.2	57.5
6	6-2	10	0.5	1735 × 16	1000 × 400, 1050 × 100	21.1	73.7
7	7-1	10	0.5	1735 × 16	1300 × 1, 1000 × 200	23.8	75.0

[a] The microstructure of this sample is heterogeneous; the reported values refer to the average size of grains in regions formed by small grains and by large grains, respectively.

not change significantly even in the case of samples containing a lower amount of TEOS (Fig. 4a).

As far as influence of the soaking time is concerned, the average grain size of pure YAG samples does not change consistently with the increase of the soaking time from 8 to 16 h. In the case of pure YAG samples, however, the microstructure is more heterogeneous, because large grains grow and small grains shrink (Table 4). Conversely, with a soaking time of only 2 h the grain size is small (around 13 compared to 21 μm of sample with 16 h of soaking time, composition with 10 at.% Yb, Table 4) and the amount of residual pores is relatively high.

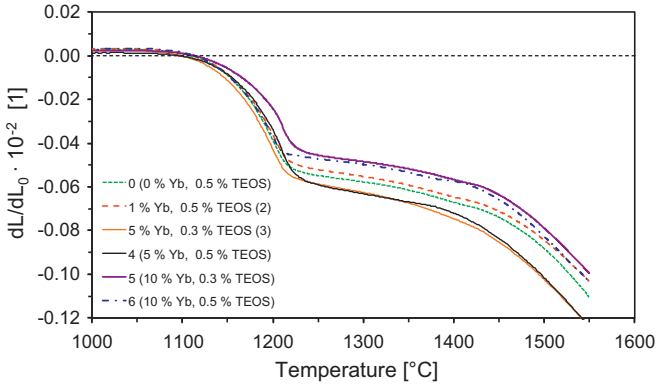

Fig. 2. Results of dilatometric analysis.

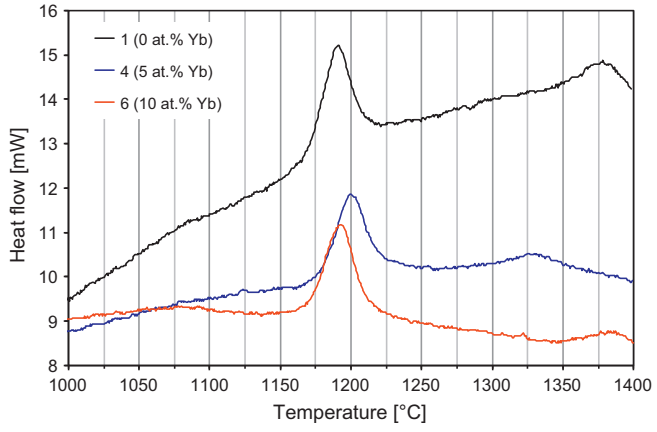

Fig. 3. Results of DTA analysis, showing the exothermic peak of YAP around 1200 °C.

The largest grain size is obtained in the case of samples containing 1 at.% Yb (28 μm, Fig. 5a). This anomalous trend can be related to what was observed during the high temperature XRD analyses, i.e. with 5 at.% Yb the YAG phase forms at low temperature and consequently it has more time to grow during sintering. Conversely, in the case of 0 and 10 at.% Yb the YAG phase forms at a higher temperature, reducing the time available for the grain growth during sintering. It can be hypothesized that in the case of samples with 1 at.% Yb the YAG phase formation temperature is even lower than with 5 at.% Yb.

The grain size is slightly larger if PEG 400 is used as dispersant instead of KM 5104, but the difference could be within the measurement error.

4.3. UV–vis transmittance

The UV–vis spectra of all samples doped with Yb exhibit the expected absorption peaks (Fig. 6a).

In terms of transmittance the sample obtained with 1 at.% Yb exhibits the highest value, which approximates 80% when sintered with the standard sintering cycle (1735 °C × 16 h) (Table 4). In case of all Yb amounts, the cycles performed with a shorter sintering time (8 or 2 h) lead to lower transmittance values than with 16 h. This result is consistent with the SEM analyses that showed the presence of a larger amount of residual pores in samples sintered for 8 and 2 h compared to 16 h (Fig. 5c).

The composition with 0.3 wt.% TEOS as silica source exhibit a lower transmittance than with 0.5 wt.% TEOS (see Fig. 6b), especially at shorter sintering times. Conversely, when samples were sintered for 16 h, the difference in transmittance values of samples obtained with 0.3 and with 0.5 wt.% TEOS was low, almost within the measurement accuracy. No obvious difference was found in the transmittance spectra of samples produced with the two dispersants, PEG or KM 5104 (see Fig. 6c).

As expected, samples with higher Yb concentration required longer annealing times to complete the oxidation of Yb and shift to transparent the green colored samples. Interestingly enough, though, also samples with lower Si content (0.3 wt.%)

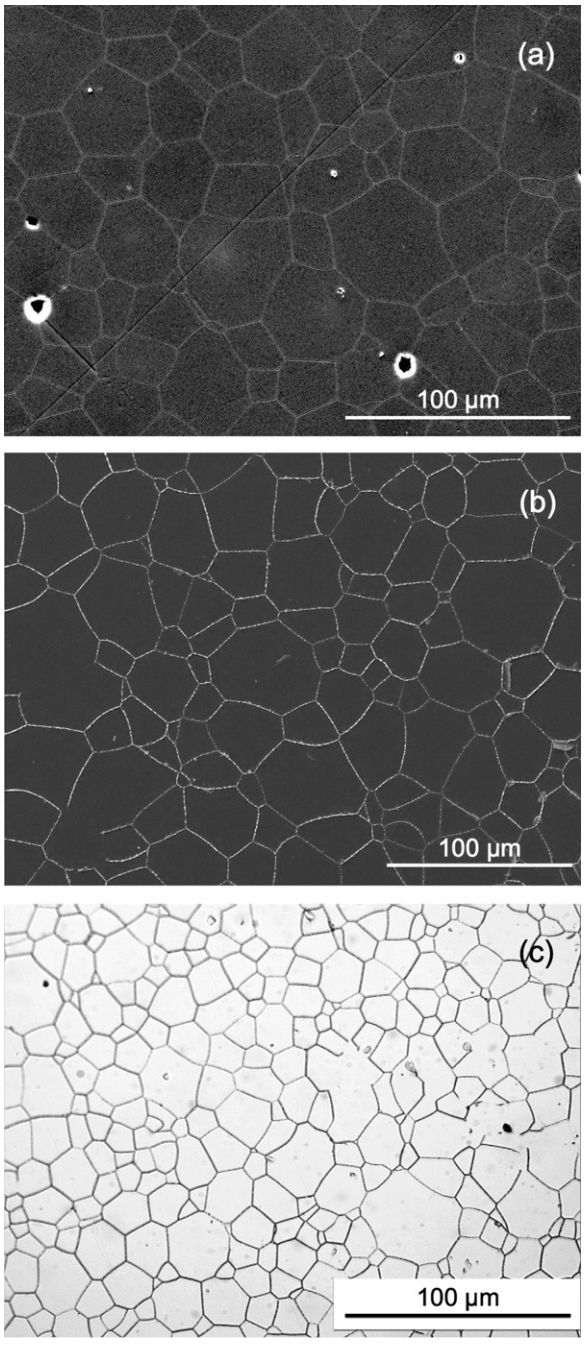

Fig. 4. Microstructure of samples containing 5 at.% of Yb; SEM micrographs of samples (a) 3-1 after etching 1400 °C × 20 min and (b) 4-1 after annealing 1100 °C × 100 h and (c) optical micrograph of sample 4-1 after aforementioned treatment.

took longer to re-oxidize compared to samples with 0.5 wt.% of TEOS after the short sintering cycle (2 h). When longer sintering times were applied (16 h), again the difference was small.

5. Discussion

The doping element (ytterbium) and sintering aid (TEOS) affected the microstructure evolution and the optical properties of sintered YAG ceramics, whereas the ytterbium concentration

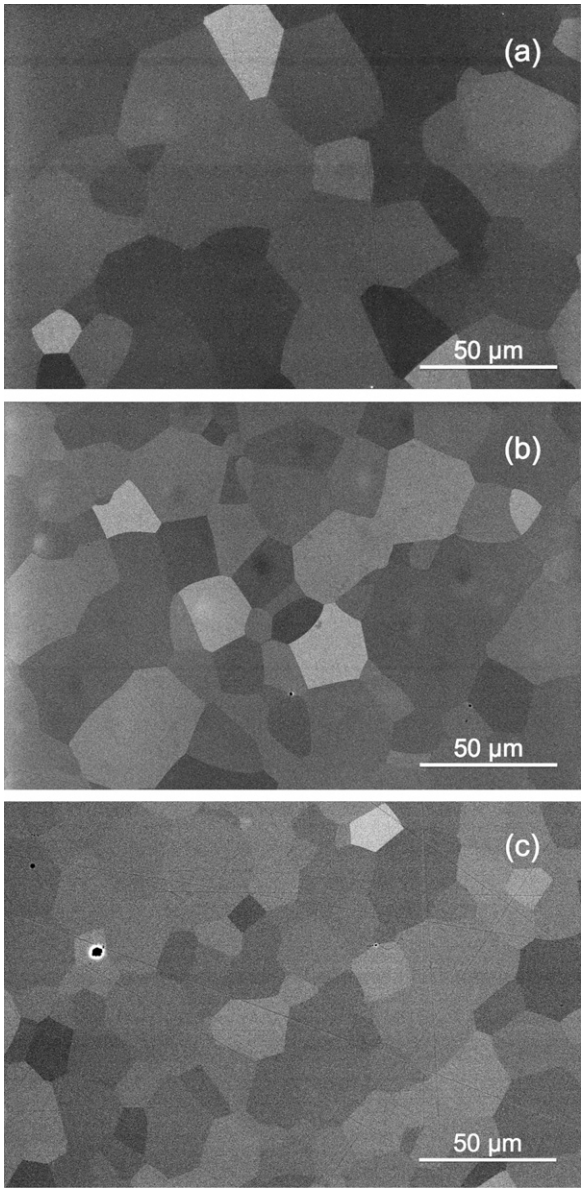

Fig. 5. ESEM micrographs of polished samples 2-1 (a) with 1 at.% Yb and 7-1 (b) with 10 at.% sintered for 16 h and sample 1-1 (c) with 0 at.% of Yb sintered for 8 h.

influenced the solid state reactions, in particular the temperature of formation of YAP and YAG phases.

The Yb content affected the optical properties, however, no clear trend could be identified, as the best UV–vis transmittance value was obtained with sample containing 1 at.% Yb, followed by 0, 10 and 5 at.%. Sample with 1 at.% Yb also exhibited the highest grain size, even though a direct relation between the grain size and transmittance among all sintered samples was not found.

According to the authors' knowledge, little has been published about effect of Yb on sintering, solid state reaction kinetics or properties of Yb:YAG,[13] and thus the more studied effect of Nd addition was taken for comparison.[25] Unlike Nd, where a direct positive effect on sintering was observed, Yb showed being neither densification-supporting, nor inhibiting.

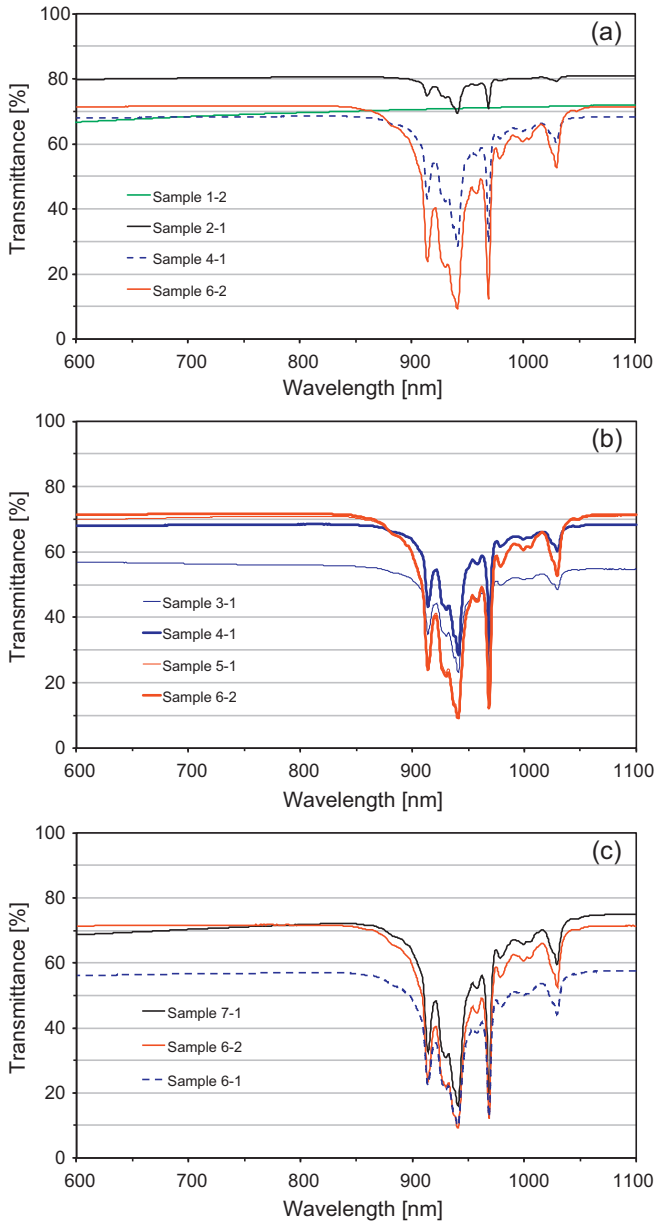

Fig. 6. UV–vis transmittance of sintered and polished samples showing the difference due to (a) Yb content, (b) Si content and (c) dispersant and sintering time.

That could be attributed to the fact that even though the Yb^{3+} ions have higher mass compared to Y^{3+} (as do the Nd^{3+} ions), and thus due to the solute drag effect[25,32] would segregate on grain boundaries, allowing the formation of secondary phases which would support liquid phase sintering, their diameter is smaller and thus they cause strain in the crystal lattice (instead of stress, as is the case of Nd^{3+}), and the tendency is to remain in the lattice instead of segregating. Also no work reports Yb segregation on grain boundaries, nor was this phenomenon observed by us via SEM and EDS. This means that although the doping principle is the same for Nd^{3+} and Yb^{3+} ions in YAG (substitution of the rare earth metals for Y^{3+} ions), the mechanisms by which the rare earth ions act on the lattice and affect the sintering process, are different. The obtained results suggest that the reason of this difference lies in the specific ion size and consequent strain–stress effects induced in the crystal lattice.

The sintering times also showed up as an important parameter. In the case of lower Si content the short sintering time (2 h) was not sufficient for the production of samples with high transmittance, and generally the residual microstructure was more disordered and exhibited more residual pores. In addition, during annealing the diffusion of oxygen is slower compared to both samples sintered for a longer time that have less residual pores and those containing more silicon; thus, a longer time is required for the complete Yb oxidation.

6. Conclusions

The high temperature data (XRD) show that, surprisingly, the addition of 5 at.% of Yb induces the formation of YAP and YAG phases at lower temperatures compared to both 0 and 10 at.% doping. Also higher shrinkage (even if not significantly) was observed for this composition at temperatures up to 1400 °C. Samples containing 1 at.% doping exhibited the highest optical transmittance (RIT 80%) and the largest average grain size (28 μm).

The decrease from 0.5 to 0.3 wt.% of TEOS affected the sintering process, the final microstructure, and in particular the optical properties of sintered material.

The results provide a clear trend of higher transmittance connected to longer sintering times, which was accentuated when the amount of Si was taken into account as shown by the significantly lower optical transmittance of samples with lower Si addition sintered for 2 h and by similar values obtained for both 0.3 and 0.5 wt.% of TEOS addition after 16 h sintering.

The results obtained so far provide evidence that for decreasing the possible amount of further phases (Si-based), longer sintering times with lower TEOS addition could be a way.

The effect of Yb on sintering and densification of Yb:YAG, as well as the effect of Si should be further studied at higher temperatures (1400–1700 °C) and in connection with the spatial distribution in the polycrystalline material via HR-TEM.

Acknowledgments

Jan Hostaša would like to thank for financial support from Specific University Research (MSMT no. 21/2011). The authors wish to thank Chiara Zanelli and Elena Landi, ISTEC CNR, for the thermal analyses and the fruitful discussions.

References

1. Krell A, Hutzler T, Klimke J. Transmission physics and consequences for materials selection, manufacturing, and applications. *J Eur Ceram Soc* 2009;**29**:207–21.
2. Taira T. Ceramic YAG lasers. *CR Phys* 2007;**8**:138–52.
3. Zhou J, Zhang W, Huang T, Wang L, Li J, Liu W, et al. Optical properties of Er, Yb co-doped YAG transparent ceramics. *Ceram Int* 2011;**37**:513–9.
4. Druon F, Balembois F, George P. New laser crystals for the generation of ultrashort pulses. *C R Phys* 2007;**8**:153–64.

5. Hönninger C, Paschotta R, Graf M, Morier-Genoud F, Zhang G, Moser M, et al. Ultrafast ytterbium-doped bulk lasers and laser amplifiers. *Appl Phys B* 1999;**69**:3–17.
6. Chénais S, Druon F, Forget S, Balembois S, Georges P. On thermal effects in solid-state lasers: the case of ytterbium-doped materials. *Prog Quantum Electron* 2006;**30**:89–153.
7. Denker B, Galagan B, Osiko V, Sverchkov S, Balbashov AM, Hellström JE, et al. Yb^{3+},Er^{3+}:YAG at high temperatures: energy transfer and spectroscopic properties. *Opt Commun* 2007;**271**:142–7.
8. Phillips JM, Coltrin ME, Crawford MH, Fischer AJ, Krames MR, Mueller-Mach R, et al. Research challenges to ultra-efficient inorganic solid-state lighting. *Laser Photonics Rev* 2007;**1**:307–33.
9. Nishiura S, Tanabe S, Fumioka K, Fujimoto Y, Nakatsuka M. Preparation and optical properties of transparent Ce:YAG ceramics for high power white LED. *IOP Conf Ser: Mater Sci Eng* 2009;**1**(012311):1–5.
10. Tsunekane M, Taira T. High-power operation of diode edge-pumped, glue-bonded, composite Yb:$Y_3Al_5O_{12}$ microchip laser with ceramic undoped YAG pump light-guide. *Jpn J Appl Phys* 2005;**44**:L1164–7.
11. Wu Y, Li J, Qiu F, Pan Y, Liu Q, Guo J. Fabrication of transparent Yb,Cr:YAG ceramics by a solid-state reaction method. *Ceram Int* 2006;**32**:785–8.
12. Chani VI, Boulon G, Zhao W, Yanagida T, Yoshikawa A. Correlation between segregation of rare earth dopants in melt crystal growth and ceramic processing for optical applications. *Jpn J Appl Phys* 2010;**49**:075601 1–756016.
13. Esposito L, Epicier T, Serantoni M, Piancastelli A, Alderighi D, Pirri A, et al. Integrated analysis of non-linear loss mechanisms in Yb: YAG ceramics for laser applications. *J Eur Ceram Soc*, doi:10.1016/j.jeurceramsoc.2012.02.047; in press.
14. Zhao W, Anghel S, Mancini C, Amans D, Boulon G, Epicier T, et al. Ce^{3+} dopant segregation in $Y_3Al_5O_{12}$ optical ceramics. *Opt Mater* 2011;**33**:684–7.
15. Esposito L, Piancastelli A, Costa AL, Serantoni M, Toci G, Vannini M. Experimental features affecting the transparency of YAG ceramics. *Opt Mater* 2011;**33**:713–21.
16. Serantoni M, Piancastelli A, Costa AL, Esposito L. Improvements in the production of Yb:YAG transparent ceramic materials: spray drying optimisation. *Opt Mater* 2012;**34**:995–1001.
17. Xu X, Zhao Z, Xu J, Deng P. Distribution of ytterbium in Yb:YAG crystals and lattice parameters of the crystals. *J Cryst Growth* 2003;**255**:338–41.
18. Bodzenta J, Kazmierczak-Balata A, Wokulska K, Kucytowski J, Szperlich P, Lukasiewicz T, et al. Analysis of influence of Yb concentration on thermal, elastic, optical and lattice parameters in YAG single crystal. *J Alloy Compd* 2009;**473**:245–9.
19. Patel AP, Levy MR, Grimes RW, Gaume RM, Feigelson RS, McClellan KJ, et al. Mechanisms of nonstoichiometry in $Y_3Al_5O_{12}$. *Appl Phys Lett* 2008;**93**:1919021–3.
20. Hess NJ, Maupin GD, Chick LA, Sunberg DS, McCreedy DE, Armstrog TR. Synthesis and crystallization of yttrium–aluminium garnet and related compounds. *J Mater Sci* 1994;**29**:1873–8.
21. Wu Y, Li J, Pan Y, Liu Q, Guo J. Synthesis of nano-sized $Yb_3Al_5O_{12}$ powders by the urea co-precipitation method. *Ceram Int* 2009;**35**:25–7.
22. Ikesue A, Yoshida K, Yamamoto T, Yamaga I. Optical scattering centers in polycrystalline Nd:YAG laser. *J Am Ceram Soc* 1997;**80**: 1517–22.
23. Boulesteix R, Maître A, Baumard JF, Rabinovitch Y, Sallé C, Weber S, et al. The effect of silica doping on neodymium diffusion in yttrium aluminum garnet ceramics: implications for sintering mechanisms. *J Eur Ceram Soc* 2009;**29**:2517–26.
24. Shannon RD, Prewitt CT. Effective ionic radii in oxides and fluorides. *Acta Crystallogr B* 1969;**25**:925–46.
25. Kochawattana S, Stevenson A, Lee S-H, Ramirez M, Gopalan V, Dumm J, et al. Sintering and grain growth in SiO_2 doped Nd:YAG. *J Eur Ceram Soc* 2008;**28**:1527–34.
26. Wen L, Sun X, Xiu Z, Chen S, Tsai C-T. Synthesis of nanocrystalline yttria powder and fabrication of transparent YAG ceramics. *J Eur Ceram Soc* 2004;**24**:2681–8.
27. Wang B, Jiang H, Jia X, Zhang Q, Sun D, Yin S. Thermal conductivity of doped YAG and GGG laser crystal. *Front Optoelectron China* 2008;**1**:138–41.
28. Jang J-W, Kim D-J, Lee DY. Size effect of trivalent oxides on low temperature phase stability of 2Y-TZP. *J Mater Sci* 2001;**36**:5391–5.
29. Krell A, Klimke J, Hutzler T. Transparent compact ceramics: inherent physical issues. *Opt Mater* 2009;**31**:1144–50.
30. Li C, Zuo H, Zhang M, Han J, Meng S. Fabrication of transparent YAG ceramics by traditional solid-state-reaction method. *Trans Nonferrous Met Soc China* 2007;**17**:148–53.
31. Chen XY, Yang L, Cook RE, Skanthakumar S, Shi D, Liu GK. Crystallization, phase transition and optical properties of the rare-earth-doped nanophosphors synthesized by chemical deposition. *Nanotechnology* 2003;**14**:670–4.
32. Cahn JW. The impurity-drag effect in grain boundary motion. *Acta Met* 1962;**10**:789–98.